ISSN (Print) 1226-1750
ISSN (Online) 2233-6656
Journal of Magnetics 22(3), 360-363 (2017) https://doi.org/10.4283/JMAG.2017.22.3.360

Effects of Octahedral Ni^{2+} on Structural and Transport Properties of $Ni_xFe_{3-x}O_4$ Thin Films

Kwang Joo Kim[1], Tae Young Koh[1], Jongho Park[1], and Jae Yun Park[2]*

[1]*Department of Physics, Konkuk University, Seoul 05029, Korea*
[2]*Department of Materials Science and Engineering, Incheon National University, Incheon 22012, Korea*

(Received 28 April 2017, Received in final form 4 July 2017, Accepted 7 July 2017)

Polycrystalline $Ni_xFe_{3-x}O_4$ thin films prepared by using a sol-gel process exhibited phase-pure spinel ($Fd\bar{3}m$) structure for the Ni composition up to x = 1.0. X-ray photoemission spectroscopy (XPS) and Raman spectroscopy investigations revealed that Ni ions mostly have valence of +2 and occupy the octahedral sites of the cationic sublattice. The $Ni_xFe_{3-x}O_4$ films exhibited higher electrical resistivity than that of Fe_3O_4 below 300 K. The increase in the resistivity is primarily ascribed to decrease in Fe^{2+}-Fe^{3+} polaronic hopping rate in the octahedral sites due to the increase in the octahedral Ni^{2+} population.

Keywords : magnetite, ferrite thin film, electrical resistivity, polaron, sol-gel

1. Introduction

The iron-oxide magnetite (Fe_3O_4) has been subject to a large number of theoretical and experimental studies due to its intriguing physical properties as well as technical applications such as power transformer, magnetic recording, magnetic refrigeration, and ferro-fluids [1-3]. The structural and magnetic properties of magnetite related to such applications can be tuned via substitution of the tetrahedral (A) or octahedral (B) cations by foreign metallic ions with little distortion of the spinel lattice. The ferrimagnetism of inverse spinel Fe_3O_4 below 860 K has been explained in terms of the antiferromagnetic spin alignment between Fe^{3+}(A) and Fe^{3+}(B) ions via the super-exchange interaction, while Fe^{2+}(B) aligns parallel to Fe^{3+}(B) via the double-exchange interaction [4]. With the magnetic moment of high-spin Fe^{3+}(A) ion being opposite to those of Fe^{3+}(B) and Fe^{2+}(B) ions, Fe_3O_4 can exhibit a net magnetic moment of ~4 μ_B per formula unit (= 500 emu/cm^3).

Despite an oxide material, Fe_3O_4 is known to have high electrical conductivity, ~10^2 Ω^{-1}cm^{-1} at temperatures near 300 K, which can be explained in terms of the polaronic electron hopping between the octahedral cations [5]. When Ni ions substitute the cationic sublattice of magnetite, the resultant $Ni_xFe_{3-x}O_4$ compounds disclosed a gradual decrease of magnetization with decreasing Ni composition [6]. In this work, the temperature dependence of electrical resistivity of $Ni_xFe_{3-x}O_4$ thin films have been measured for the Ni composition up to x = 1.0. Although majority of research on ferrites tend to be populated on powder samples, film samples are more advantageous for accurate measurements of the inherent properties of granular oxides such as electrical resistivity, optical absorption, and photoemission.

The structural properties of the present sol-gel prepared $Ni_xFe_{3-x}O_4$ thin films were investigated by X-ray diffraction (XRD) and Raman spectroscopy. The ionic valences of Fe and Ni ions in $Ni_xFe_{3-x}O_4$ were investigated by X-ray photoemission spectroscopy (XPS). The electrical resistivity of the $Ni_xFe_{3-x}O_4$ samples was measured at varying temperature in order to investigate the variation in polaronic conductivity with Ni doping.

2. Experimental

The present $Ni_xFe_{3-x}O_4$ films were fabricated by using a sol-gel process wherein the precursor solution was prepared by dissolving $Fe(NO_3)_3 \cdot 9H_2O$ and $Ni(CH_3CO_2)_2 \cdot 4H_2O$ powders together in 2-methoxyethanol at 160 °C. The substrate, α-Al_2O_3(0001), was spin-coated by the precursor solution at 3000 rpm for 20 s and then heated at 300 °C

*Corresponding author: Tel: +82-32-835-8271
Fax: +82-32-835-0778, e-mail: pjy@inu.ac.kr

for 4 min. This process was repeated for increasing the film thickness. For the present $Ni_xFe_{3-x}O_4$ films with phase purity, post-annealing was performed in evacuated (~10^{-3} Torr) quartz tube at 800 °C for 4 h.

The thickness of the magnetic films estimated by using scanning electron microscopy was in the 0.6-0.8 μm range. The crystalline structure of the samples was monitored by using XRD (Cu K_α line) in the grazing-incidence geometry with fixed X-ray incidence angle of 4°. XPS measurements were performed using the Al K_α line in order to find preferred valence of Ni and Fe ions in the oxides. Raman spectra of the specimens were measured using an Ar-ion laser (wavelength = 514 nm) at room temperature. Temperature-dependent DC electrical resistivity measurements were performed on bar-shaped (1 mm wide and 10 mm long) samples in the 100-300 K range by using a ^{4}He cryostat (PPMS-9, Quantum Design™, San Diego, CA, USA). At each temperature (T) step (ΔT = 1 K), the measurement was performed under a current supply of 1 mA after the temperature had stabilized.

3. Results and Discussion

The XRD patterns of the sol-gel prepared polycrystalline $Ni_xFe_{3-x}O_4$ ($x \leq 1.0$) films are exhibited in Fig. 1. All the diffraction peaks could be indexed based on a spinel phase (cubic space group $Fd\bar{3}m$; JCPDS 88-0866) regardless of the Ni composition (x). The XRD peaks of the $Ni_xFe_{3-x}O_4$ samples shift to larger angles with increasing x as shown by a dashed line near the (440) peak, indicating a gradual decrease of the lattice parameter of $Ni_xFe_{3-x}O_4$. For the Fe_3O_4 film, the calculated cubic lattice parameter is 0.8385 nm, which is in agreement with a bulk lattice parameter (0.8385 nm in JCPDS 88-0866). The lattice parameters of the $Ni_xFe_{3-x}O_4$ films are 0.8370, 0.8347, 0.8317, and 0.8299 nm for x = 0.2, 0.4, 0.6, and 0.8, respectively. However, for x = 1.0, new peaks appear near (311), (400), (511), and (440) peaks as marked by arrows in Fig. 1. It can be understood in terms of a tetragonal distortion of the unit cell at large Ni compositions.

In Fig. 2(a), the Ni 2p-electron binding-energy (BE) spectra of the $Ni_xFe_{3-x}O_4$ samples obtained by XPS measurements are exhibited. The emission peaks near 854 and 872 eV (marked by arrows) are identified as the spin-orbit-split $2p_{3/2}$ and $2p_{1/2}$ peaks, respectively, from ionic Ni with valence of +2. The peak near 861 eV (marked by asterisk) is identified as a major satellite to the $2p_{3/2}$ emission from octahedral Ni^{2+} ions [7, 8]. Thus, the Ni 2p XPS spectra indicate dominance of octahedral Ni^{2+} ions in the $Ni_xFe_{3-x}O_4$ samples. In Fig. 2(b), the Fe 2p-electron BE spectra of the $Ni_xFe_{3-x}O_4$ samples show that the main $2p_{3/2}$ peak can be resolved by two contributions, Fe^{2+} near 709 eV and Fe^{3+} near 711 eV as marked by arrows. The photoelectron spectral shapes for the present $Ni_xFe_{3-x}O_4$ samples are well distinguishable from those for iron oxides

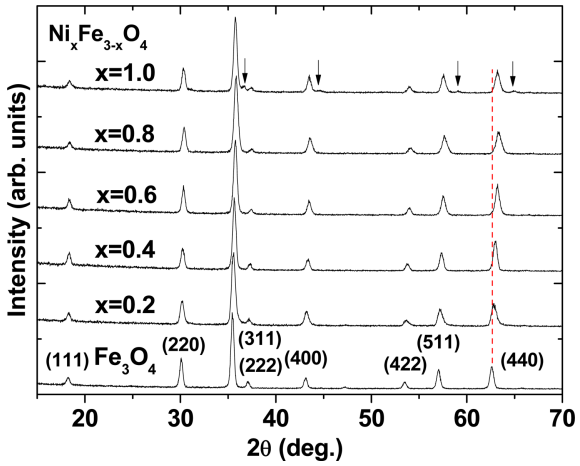

Fig. 1. (Color online) X-ray diffraction patterns of polycrystalline $Ni_xFe_{3-x}O_4$ films.

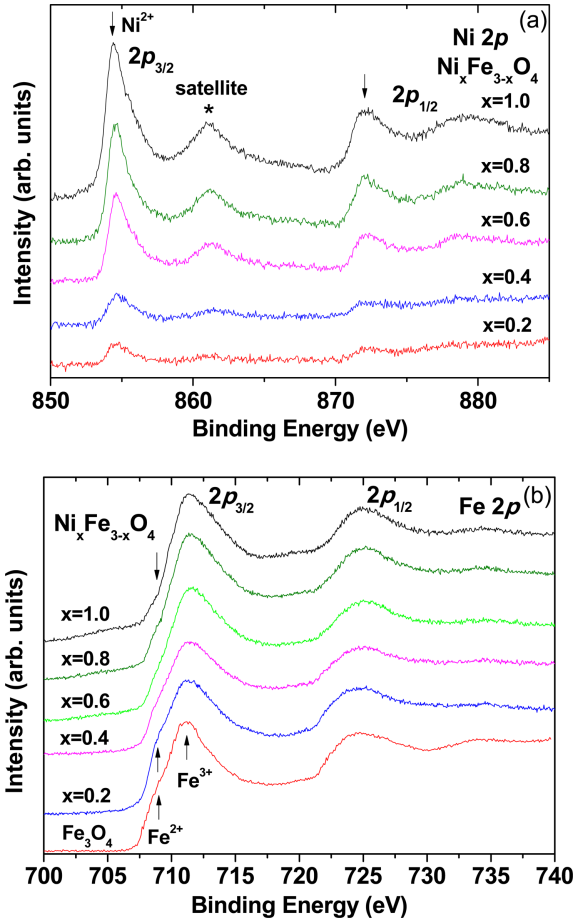

Fig. 2. (Color online) X-ray photoemission spectra of (a) Ni 2p and (b) Fe 2p electrons of polycrystalline $Ni_xFe_{3-x}O_4$ films.

containing Fe^{3+} ions only [9, 10]. For the $Ni_xFe_{3-x}O_4$ samples, the Fe^{2+} strength is seen to become weaker with increasing x compared to that of Fe_3O_4, suggesting a decrease in the octahedral Fe^{2+} concentration caused by the Ni^{2+} substitution. The octahedral preference of the Ni ions has been reported in a number of study on spinel oxides [11, 12]. The decrease of the lattice parameter for $Ni_xFe_{3-x}O_4$ with increasing x as indicated by the XRD data (Fig. 1) can be explained in terms of the smaller ionic radius of high-spin Ni^{2+} ion (0.069 nm) than that of high-spin Fe^{2+} ion (0.078 nm) in the octahedral site.

In Fig. 3, the Raman spectra of the nickel-ferrite samples are exhibited in comparison with that of Fe_3O_4. The Raman spectrum of the Fe_3O_4 sample exhibits a prominent peak near 667 cm^{-1}, which is assigned to the A_{1g} phonon mode associated with symmetric stretching of oxygen in the tetrahedral (AO_4) sites [13, 14]. For the $Ni_xFe_{3-x}O_4$ samples, the corresponding Raman peak shifts to the higher energies with increasing x (704 cm^{-1} for x = 1.0) compared to that of Fe_3O_4 as denoted by arrows. It is seen that the A_{1g} peak maintains similar lineshape for all the samples, implying that the tetrahedral sites are hardly occupied by foreign (Ni^{2+}) ions, thus, supporting the octahedral preference of the Ni^{2+} ions. It is also seen that the Raman peak near 540 cm^{-1} for Fe_3O_4, being ascribed to one of the three T_{2g} modes associated with asymmetric stretching of oxygen in the AO_4 sites, gets stronger and gradually shifts to higher energies with increasing x (580 cm^{-1} for x = 1.0) as in the A_{1g} mode. Such high-energy shift of the two phonon modes for $Ni_xFe_{3-x}O_4$ is interpreted as due to the increase of the A-O bond strength [15] caused by the decrease of the lattice parameter of the nickel-ferrites compared to that of Fe_3O_4. A Raman peak appearing near 330 cm^{-1} at large Ni compositions ($x \geq 0.6$) is ascribed to the E_g mode associated with symmetric bending of the tetrahedral O^{2-} ions. There is another Raman peak prominent at large Ni compositions near 480 cm^{-1} (denoted as α). It was interpreted as due to excitation of magnons [15, 16].

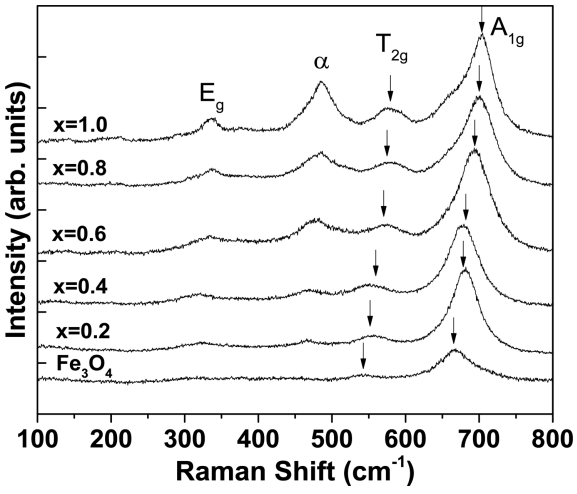

Fig. 3. Raman shifts of polycrystalline $Ni_xFe_{3-x}O_4$ films.

In Fig. 4(a), the electrical resistivity (ρ) data of the $Ni_xFe_{3-x}O_4$ films are exhibited. All the specimens show decreasing ρ with increasing T that can be observed for usual non-metallic materials. The electrically insulating α-Al_2O_3(0001) substrate seldom affect the measurement of ρ. It is also seen that ρ of the $Ni_xFe_{3-x}O_4$ films gets larger with increasing x at all temperatures. At T = 300 K, ρ is as low as 1.6×10^{-1} Ω·cm for Fe_3O_4, while it is 1.4×10^{1} Ω·cm for x = 1.0, thus, being increased by a factor of ~10^2. The increase in the resistivity of the $Ni_xFe_{3-x}O_4$ samples compared to that of Fe_3O_4 can be understood in terms of the decrease of thermally-activated d-electron hopping rate between $Fe^{2+}(d^6)$ and $Fe^{3+}(d^5)$ ions in the

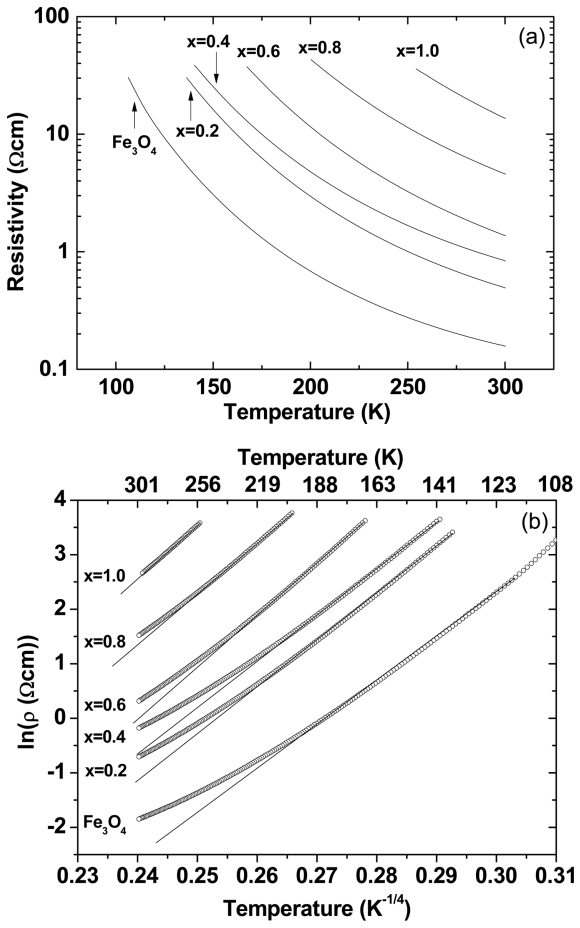

Fig. 4. (a) Temperature dependence of DC electrical resistivity ρ of $Ni_xFe_{3-x}O_4$ films. (b) Dependence of ln(ρ) on $T^{-1/4}$. The experimental data are denoted as open circles. The straight lines drawn along with the experimental data are obtained by least-squares fittings on linear region of the data points.

octahedral sites of the spinel lattice [11, 17]. Such electron-hopping conduction in ionic crystals has been theoretically explained in terms of polaron, a virtual particle composed of an electron and surrounding phonons [18]. In inverse-spinel Fe_3O_4 where the octahedral sites are occupied by equal quantity of Fe^{2+} donors and Fe^{3+} acceptors, the donor-acceptor pairs for the polaronic transport exist in abundance. The decrease in the octahedral Fe^{2+} quantity through Ni^{2+} substitution in $Ni_xFe_{3-x}O_4$ leads to a decrease in Fe^{2+}-Fe^{3+} pairs, resulting in the decrease in electrical conductivity.

Considering the polaron as originating from Coulomic electron-phonon interaction, the decreasing resistivity with increasing T can be explained in terms of the increase in the phonon population and the resultant increase in the polaronic Fe^{2+}-Fe^{3+} hopping probability. The temperature dependence of electrical properties caused by polaronic hopping can be described as

$$\ln\left(\frac{\rho}{\rho_0}\right) = \left(\frac{T_0}{T}\right)^q$$

wherein the exponent q is variable as q = 1 for nearest-neighbor hopping (NNH) and q = 1/4 for variable-range hopping (VRH), and ρ_0 and T_0 are constants [18, 19]. Thus, in Fig. 4(b), the plots of ln(ρ) of the $Ni_xFe_{3-x}O_4$ films on $T^{-1/4}$ are exhibited. The ln(ρ) data are seen to vary in quite linear manner with $T^{-1/4}$ at low temperatures. The linear part of the ln(ρ) *vs.* $T^{-1/4}$ plot in the low temperature region was least-squares fitted as denoted by straight line in in Fig. 4(b). The x = 0.2, 0.4, and 0.6 samples show good linearity up to ~220 K. On the other hand, such linear behavior was not observed for the ln(ρ) *vs.* T^{-1} relation of the samples in the same temperature range. Thus, the analysis on the temperature dependence of ln(ρ) implies that the polaronic transport of Fe d electrons in $Ni_xFe_{3-x}O_4$ is better explained by the VRH model than the NNH model at low temperatures.

4. Conclusions

Polycrystalline $Ni_xFe_{3-x}O_4$ ($x \leq 1.0$) thin films prepared by sol-gel process exhibit phase purity and decrease of lattice parameter with increasing Ni composition. XPS and Raman investigations reveal that the Ni ions in $Ni_xFe_{3-x}O_4$ have valence of +2 and occupy octahedral sites mostly. The electrical resistivity data for the $Ni_xFe_{3-x}O_4$ films exhibit $T^{-1/4}$ dependence at low temperatures (< 220 K), implying VRH-type polaronic transport. The decrease in the octahedral Fe^{2+} population and the resultant decrease in the Fe^{2+}-Fe^{3+} hopping probability by the Ni doping is ascribed to the main reason for the gradual increase in the resistivity with increasing x.

Acknowledgment

This work was supported by Incheon National University Research Grant in 2015.

References

[1] A. Goldman, Modern Ferrite Technology, Springer, New York (2006).
[2] U. B. Gawas, V. M. S. Verenkar, S. R. Barman, S. S. Meena, and P. Bhatt, J. Alloys Comp. **555**, 225 (2013).
[3] Q. Liu, Z. Zi, M. Zhang, A. Pang, J. Dai, and Y. Sun, J. Alloys Comp. **561**, 65 (2013).
[4] M. Ishikawa, H. Tanaka, and T. Kawai, Appl. Phys. Lett. **86**, 222504 (2005).
[5] S. B. Ogale, K. Ghosh, R. P. Sharma, R. L. Greene, R. Ramesh, and T. Venkatesan, Phys. Rev. B **57**, 7823 (1998).
[6] K. J. Kim, M. H. Kim, and C. S. Kim, J. Magn. **19**, 111 (2014).
[7] S. Altieri, L. H. Tjeng, A. Tanaka, and G. A. Sawatzky, Phys. Rev. B **61**, 13403 (2000).
[8] S. Ivanova, E. Zhecheva, R. Stoyanova, D. Nihtianova, S. Wegner, P. Tzvetkova, and S. Simova, J. Phys. Chem. C **115**, 25170 (2011).
[9] T. Fujii, F. M. F. de Groot, G. A. Sawatzky, F. C. Voogt, T. Hibma, and K. Okada, Phys. Rev. B **59**, 3195 (1999).
[10] K. J. Kim, J. H. Lee, and C. S. Kim, J. Kor. Phys. Soc. **61**, 1274 (2012).
[11] A. K. Singh, T. C. Goel, and R. G. Mendiratta, Solid State Commun. **125**, 121 (2003).
[12] M. Sertkol, Y. Koseoglu, A. Baykal, H. Kavas, and A. C. Basaran, J. Magn. Magn. Mater. **321**, 157 (2009).
[13] Z. Wang, R. T. Downs, V. Pischedda, R. Shetty, S. K. Saxena, C. S. Zha, Y. S. Zhao, D. Schiferl, and A. Waskowska, Phys. Rev. B **68**, 094101 (2003).
[14] O. N. Shebanova and P. Lazor, J. Solid State Chem. **174**, 424 (2003).
[15] R. Gupta, A. K. Sood, P. Metcalf, and J. M. Honig, Phys. Rev. B **65**, 104430 (2002).
[16] L. Degiorgi, I. Blatter-Morke, and P. Wachter, Phys. Rev. B **35**, 5421 (1987).
[17] P. P. Hankare, K. R. Sanadi, K. M. Garadkar, D. R. Patil, and I. S. Mulla, J. Alloys Comp. **553**, 383 (2013).
[18] R. Schmidt, A. Basu, and A. W. Brinkman, Phys. Rev. B **72**, 115101 (2005).
[19] A. Karmakar, S. Majumdar, and S. Giri, Phys. Rev. B **79**, 094406 (2009).